Published in final edited form as:
J Comput Assist Tomogr. 2008 ; 32(5): 750–756. doi:10.1097/RCT.0b013e31816a6823.

Receiver Operating Characteristic Analysis of Diffusion-Weighted Magnetic Resonance Imaging in Differentiating Hepatic Hemangioma From Other Hypervascular Liver Lesions

Josephina A. Vossen, MD[*], **Manon Buijs, MD**[*], **Eleni Liapi, MD**, **John Eng, MD**, **David A. Bluemke, MD, PhD**, and **Ihab R. Kamel, MD, PhD**
Russell H. Morgan Department of Radiology and Radiological Sciences, Johns Hopkins Hospital, Baltimore, MD

Abstract

Purpose—To evaluate the role of diffusion-weighted imaging in differentiating between hepatic hemangiomas, both typical and atypical, and other hypervascular liver lesions.

Methods—Retrospective review of 182 hypervascular liver lesions in 117 patients was performed. Diffusion and contrast-enhanced magnetic resonance imaging were performed using a 1.5-T unit. Imaging protocol consisted of T_2-weighted fast spin-echo images, breath-hold diffusion-weighted echo-planar images, and breath-hold unenhanced and contrast-enhanced T_1-weighted 3-dimensional fat-suppressed spoiled gradient-echo images in the arterial phase (20 seconds) and portal venous phase (60 seconds). Signal intensity changes and apparent diffusion coefficient (ADC) values were evaluated for all lesions. Unpaired *t* test was used to compare the mean ADC values for different lesions, and statistical significance was set at $P < 0.01$. Receiver operating characteristic analysis was used to determine the accuracy of diffusion-weighted imaging in differentiating hemangiomas from other hypervascular liver lesions.

Results—Lesions included typical and atypical hemangioma (n = 38), hepatocellular carcinoma (HCC; n = 58), focal nodular hyperplasia (FNH; n = 22), and neuroendocrine tumor metastasis (NET; n = 64) with a mean tumor size of 5.3 cm. Mean ADC value for hemangioma, HCC, FNH, and NET was 2.29×10^{-3}, 1.55×10^{-3}, 1.65×10^{-3}, and 1.43×10^{-3} mm^2/s, respectively. There was a statistically significant difference in the ADC value of hemangioma compared with that of FNH ($P < 0.001$), HCC ($P < 0.001$), and NET ($P < 0.001$), respectively. The area under the receiver operating characteristic curve was 0.91.

Conclusions—Diffusion-weighted magnetic resonance imaging and ADC maps can provide rapid quantifiable information to differentiate typical and atypical hemangiomas from other hypervascular liver lesions.

Keywords

diffusion imaging; liver lesion; MR imaging

Diffusion-weighted (DW) magnetic resonance (MR) imaging and apparent diffusion coefficient (ADC) values map the thermally induced motion of water molecules in biologic

Reprints: Ihab R. Kamel, MD, PhD, Russell H. Morgan Department of Radiology, and Radiological Sciences, 601 N Caroline St, Rm 3235A, Baltimore, MD 21287 (ikamel@jhmi.edu)..

[*]J.A. Vossen and M. Buijs contributed equally to this work.

tissues, known as Brownian motion, and are thereby able to provide insight into tumor microstructure.[1,2] The motion includes not only molecular diffusion of water but also microcirculation of blood (microperfusion). The primary application of diffusion-weighted imaging (DWI) has been in brain imaging.[3-5] More recently, DWI has been used to characterize focal hepatic lesions.[6-10] However, the accuracy of DWI in the differentiation between hepatic hemangioma and other hypervascular lesions remains unknown.

Hemangioma is the most common benign hepatic tumor, occurring in 5% to 20% of the population.[11,12] Typical hemangiomas are less than 3 cm in size and are usually spheroid or ovoid. On nonenhanced computed tomography (CT) images, hemangiomas typically appear as a low attenuating lesion.[13,14] On T_1-weighted MR images, hemangiomas characteristically appear as hypointense lesions, and on T_2-weighted MR images, they are extremely hyperintense. After administration of an intravenous contrast, CT and dynamic MR imaging demonstrate peripheral nodular enhancement in the early phase. Venous-phase imaging shows centripetal enhancement that progresses to uniform filling. This enhancement persists on delayed-phase images.[15,16]

Although atypical hemangiomas are less common, they are clinically important, because their differential diagnosis includes a large variety of liver tumors.[17] Clinically relevant atypical hemangiomas include large heterogeneous hemangiomas, calcified hemangiomas, pedunculated hemangiomas, and hemangiomas developing in diffuse fatty liver.[5,18-20] On imaging, these atypical hemangiomas may resemble malignant liver lesions, such as hepatocellular carcinoma (HCC), hypervascular liver metastases, or occasionally, other benign lesions such as focal nodular hyperplasia (FNH).

It is essential for physicians to accurately differentiate between hemangiomas and other liver lesions to determine future therapy and prognosis. Presently, CT and MR imaging are the mainstay for detection and characterization of liver tumors.[21-27] It has been reported that contrast-enhanced MR imaging is more sensitive in detecting and more useful in characterizing focal hepatic lesions than CT.[28-31] However, there is a growing interest in the role of DWI in characterizing hepatic lesions.

Therefore, the aim of this study was to perform receiver operating characteristic (ROC) analysis of the accuracy of DWI in the differentiation between hepatic hemangiomas and other hypervascular liver lesions more than 1 cm in size.

MATERIALS AND METHODS

Patients

Between January 2003 and January 2005, we reviewed all patients with MR imaging studies performed for the characterization of 1 or more liver lesions. The following patients were included in our study: (1) those who had 1 or more hypervascular liver lesions, including hemangioma, FNH, HCC, and hypervascular liver metastases; (2) those who had liver lesions with the size of more than 1 cm to be detected by DWI. The confirmation criteria for typical hemangioma were characteristic findings on dynamic-enhanced MR imaging (high signal intensity on T_2-weighted images and marked and progressive nodular enhancement) with a minimum of 1 year of follow-up, showing stability in size and morphology. The confirmation criteria for atypical hemangioma were pathological proof or dynamic-enhanced MR imaging with a minimum of 2 years of follow-up, showing stability in size and morphology. The confirmation criteria for FNH were typical findings on MR imaging (ie, isointensity on T_1- and T_2-weighted images with a central scar, homogeneous enhancement in the hepatic arterial phase, and isointense to the liver in the portal venous phase). The confirmation criteria for FNH presenting without a central scar were stability in size and morphology (ie, isointensity on

T_1- and T_2-weighted images, homogeneous enhancement in the hepatic arterial phase, and isointense to the liver in the portal venous phase) for more than 2 years or tissue biopsy. The diagnosis of HCC was based on either histology obtained by needle biopsy or a single hypervascular lesion on MR imaging in addition to an α-fetoprotein level greater than 400 in a cirrhotic patient. All hypervascular metastases were diagnosed by biopsy of a representative liver lesion. This retrospective review was approved by our institutional review board. One experienced MR radiologist not involved in the image analysis reviewed the clinical reports, collected demographic information, histopathologic, and imaging findings, and identified 117 patients who met the inclusion criteria. Up to 5 lesions per patient were evaluated, resulting in a total of 182 lesions.

Magnetic Resonance Imaging Technique

Patients were scanned using a 1.5-T MR scanner (CV/i; General Electric Medical Systems, Milwaukee, Wis) and a phased-array torso coil. Imaging protocol included T_2-weighted fast spin-echo (SE) images (matrix, 256 × 256; slice thickness, 8 mm; interslice gap, 2 mm; repetition time [T_R], 5000 milliseconds; echo time [T_E], 100 milliseconds; receiver bandwidth, 32 kHz), breath-hold diffusion-weighted echo-planar images (matrix, 128 × 128; slice thickness, 8 mm; interslice gap, 2 mm; *b* value, 500 mm^2/s; T_R, 5000-6500 milliseconds; T_E, 110 milliseconds; receiver bandwidth, 32 kHz), and breath-hold unenhanced and contrast-enhanced (0.1 mmol/kg intravenous gadodiamide; Omniscan; Amersham, Princeton, NJ) T_1-weighted 3-dimensional fat-suppressed spoiled gradient-echo images (field of view, 320-400 mm; matrix, 192 × 160; slice thickness, 4 T_E, 1.2 milliseconds; receiver bandwidth, 64 kHz; flip angle, 15 degrees) in the arterial (20 seconds) and portal venous (60 seconds) phases.

Image Analysis

Magnetic resonance image processing and ADC maps were generated using a commercially available Advantage Windows workstation (General Electric Medical Systems). Images were interpreted by consensus of 2 experienced MR radiologists, who were blinded to the diagnosis at the time of evaluation of the DW images. The reviewers were not provided with the conventional images. Parameters evaluated included signal intensity changes and ADC values. For patients with more than 1 lesion, all lesions of 1 cm or larger were evaluated, up to a maximum of 5 lesions to ensure independent sampling. Apparent diffusion coefficient maps were generated from the DW images, and values were recorded by placing a region of interest over the entire lesion, as seen on the image with the largest lesion size.

Statistical Analysis

Statistical analysis was performed with the Stata software package (version 8; Stata Corp, College Station, Tex). Mean ADC values of the 4 lesion types (hemangioma, HCC, FNH, neuroendocrine tumor metastasis [NET]) were compared with multinomial logistic regression using robust variance estimation to account for potential correlation of multiple lesions within the same patient. Mean ADC values of classic versus atypical hemangiomas were compared with an unpaired *t* test. $P < 0.01$ were considered statistically significant. An ROC curve was constructed to summarize the trade-off between sensitivity and specificity of different threshold ADC values that may be chosen to separate hemangiomas from the other lesion types. The nonparametric (trapezoidal rule) area under the ROC curve was calculated to represent the overall accuracy.

RESULTS

Demographic Information

General information for all 117 patients (68 men and 49 women) is shown in Table 1. A total of 182 hypervascular lesions were evaluated. The mean number of evaluated lesions per patient was 1.5 (range, 1-5). The lesions were diagnosed as either hemangioma (n = 38), HCC (n = 58), FNH (n = 22), or NET (n = 64). Mean tumor size on MR imaging was 5.3 cm (range, 1.0-17.8 cm).

Findings on MR Imaging

A total of 25 hemangiomas had characteristic findings on unenhanced (high signal intensity on T_2-weighted images) and dynamic-enhanced (marked and progressive nodular enhancement) MR imaging (Fig. 1) and remained stable in size and morphology at 1 year. The remaining 13 hemangiomas were classified as atypical, 7 were diagnosed as giant (>4 cm) hemangiomas on MR imaging, and the remaining 6 hemangiomas had an atypical enhancement pattern. Four of 6 atypical lesions did not fill on delayed images (Fig. 2), and 2 lesions showed complete filling in the arterial phase (flash filling) that persisted on delayed images (Fig. 3). The diagnosis was confirmed histologically in 2 of 13 atypical lesions. The remaining 11 lesions remained stable on MR imaging at 2 years.

All NETs were hyperintense on T_2-weighted images and were hypervascular in the arterial phase. All FNH lesions showed homogeneous enhancement in the arterial phase and became isointense to the liver in the portal venous phase. A central scar that was bright on T_2 was present in 14 (64%) of 22 lesions. Thirty-seven (64%) of 58 HCCs were found in patients with underlying cirrhosis. The remaining 21 lesions (36%) developed in noncirrhotic livers. In these patients, biopsy confirmed the diagnosis of HCC.

Findings on DW MR Imaging

On DW MR imaging, all 38 hemangiomas (100%) were markedly hyperintense compared to surrounding liver parenchyma. Most HCC lesions (n = 45; 78%) were slightly hyperintense relative to the surrounding liver parenchyma. The remaining lesions were either markedly hyperintense (10 lesions; 17%) or isointense (3 lesions; 5%) to surrounding liver parenchyma. Of 22 FNH lesions, 20 were slightly hyperintense, and 2 were isointense to surrounding liver parenchyma. All except for 1 of NETs were markedly hyperintense (Table 2).

After drawing a region of interest on the ADC maps, the mean ADC value for hemangioma, HCC, FNH, and NET was 2.29×10^{-3}, 1.55×10^{-3}, 1.65×10^{-3}, and 1.43×10^{-3} mm^2/s, respectively (Table 3). Multinomial logistic regression demonstrated a statistically significant difference between ADC values for hemangiomas and all other hypervascular lesions (FNH, HCC, and NET) ($P < 0.001$). Statistical significance was maintained even when considering classic and atypical hemangiomas separately. No statistically significant difference was found between the ADC values of classic hemangiomas and of atypical ones ($P = 0.99$). No statistically significant difference was found between the ADC values of HCC in cirrhotic and those of noncirrhotic livers ($P = 0.38$).

Furthermore, ROC analysis demonstrated an area under the curve of 0.91, indicating that DW MR imaging is good at correctly classifying hemangiomas from the other hypervascular liver lesions (Fig. 4). As in all tests summarized by an ROC curve, the optimum operating point (sensitivityspecificity pair) along the ROC curve will depend on the particular clinical circumstances and the utilities assigned to the possible clinical outcomes. Scatterplot of the ADC values of all lesions is shown in Figure 5. Apparent diffusion coefficient values were very accurate when a threshold value of 2.30×10^{-3} mm^2/s was used, correctly categorizing

21 (55%) of 38 hemangiomas, and missing no other hypervascular liver lesions with a sensitivity of 55% (confidence interval [CI], 38%-71%), a specificity of 100% (CI, 97%-100%), a positive predictive value of 100% (CI, 81%-100%), and a negative predictive value of 89% (CI, 83%-94%). A threshold of 2.00×10^{-3} mm^2/s included 29 of 38 hemangiomas, but misclassified 4 NET, 1 HCC, and 1 FNH, if only the ADC values were considered in the diagnosis, with a sensitivity of 76% (CI, 59%-88%), a specificity of 96% (CI, 91%-98%), a positive predictive value of 83% (CI, 66%-93%), and a negative predictive value of 94% (CI, 88%-97%). All lesions with an ADC value below 1.17×10^{-3} mm^2/s were malignant.

DISCUSSION

Diffusion is the random microscopic translation motion of water molecules, known as Brownian motion. By applying 2 motion-probing gradients before and after the 180-degree pulse, MR imaging can be made sensitive to the diffusion of water molecules in tissue. The combined motion effects of both capillary perfusion and diffusion are quantified by means of the ADC value.[32] The initial applications of DW MR imaging have been in brain imaging, mainly for the evaluation of acute ischemic stroke, intracranial tumors, and demyelinating disease.[33,34] The ultrafast echo-planar imaging technique has broadened the clinical use of DW MR imaging to other organs, such as the liver. Several studies showed that DWI can be used to identify and characterize focal hepatic lesions.[9,10,35,36]

Because of the high prevalence of hemangiomas in the general population, differentiation between hemangiomas and other hypervascular liver lesions is of great clinical importance. Several techniques of image acquisition and analysis have been used to evaluate liver lesions. These techniques include dynamic contrast-enhanced imaging and moderately T_2-weighted SE images, heavily T_2-weighted SE images, moderately T_2-weighted fast SE images, and dual-echo images, performed with conventional SE, half Fourier-acquired singleshot turbo SE (HASTE), and echo-planar imaging.[26] In the evaluation of T_2-weighted images, both quantitative and qualitative analyses may be used.[37-40] However, the quantitative measurement of T_2 relaxation times is significantly better than that of the subjective visual assessment, resulting in a more accurate differentiation between hepatic lesions. However, the value of DWI is not yet established.

Although most hemangiomas have typical imaging characteristics, atypical hemangiomas are clinically important, because they often resemble malignant liver lesions. Heterogeneous giant hemangiomas (>4 cm in diameter) have a differential diagnosis that includes all malignant liver lesions with a scar, such as FNH and HCC.[18] Diffuse fatty infiltration of the liver may alter the typical appearance of hepatic lesions including hemangioma.[20] With progressive cirrhosis, hemangiomas are likely to decrease in size and become more fibrotic.[41]

Focal nodular hyperplasia is the second most common benign hepatic tumor.[11] On MR imaging, FNH is usually isointense on T_1-weighted images and slightly hyperintense on T_2-weighted images. A central scar, which is typical for FNH, can be seen on T_1- and T_2-weighted images. On contrastenhanced MR imaging, because of their prominent vascularity, FNH lesions tend to enhance homogeneously with marked hyperintensity in the hepatic arterial phase and usually become isointense to liver parenchyma in the portal venous phase.[42]

Hepatocellular carcinoma is the fifth most common cancer in the world and represents more than 5% of all cancers.[43] On T_1-weighted MR images, HCC is frequently observed as hypointense, but depending on fat content, copper deposition, and protein content, it can range from hypointense to hyperintense. On T_2-weighted images, HCC is normally observed as hyperintense. After administration of a contrast, enhancement in the arterial phase and

heterogeneous washout in the portal venous phase are typical findings for HCC.[44] Hepatocellular carcinoma developing in a cirrhotic liver is commonly seen and easily recognized by radiologists. However, HCC occurring in a noncirrhotic liver may be difficult to distinguish from other hypervascular liver lesions,[45,46] and therefore, DW imaging may be of value in such cases.

The aim of our study was to assess the usefulness of DW MR imaging in this serious matter. In our study, we tested the accuracy of DW MR imaging in differentiating between hemangiomas and other relatively common hypervascular liver lesions, including FNH, HCC, and hypervascular liver metastases. There are several advantages for using DW sequences over conventional acquisitions. These echo-planar acquisitions are obtained in a breath-hold, and the ADC values generated provide quantifiable information that can be statistically analyzed. Moreover, this information is independent on the dynamics of contrast enhancement, and therefore can be easily reproduced. Furthermore, DWI can be used in those patients where contrast images cannot be obtained. An important category of patients for whom the use of intravenous contrast is contraindicated are those patients with nephrogenic systemic fibrosis. In these patients, T_2 images alone can prove difficult to interpret, and adding DW imaging would improve diagnostic success. Our results showed that the difference between ADC values for hemangioma and for all other evaluated hypervascular lesions was statistically significant ($P < 0.001$). However, our results slightly differed from those found by Quan et al[10] and Sun et al.[47] These differences might be explained by the fact that the generated ADC values are equipment-specific. Furthermore, the ROC analysis showed an area under the curve of 0.91 for differentiating hemangioma from all other observed hypervascular liver lesions, indicating that DW MR imaging can be of great value. On the basis of the ADC measurements, we can expect certain sensitivity and specificity in making the diagnosis of hemangioma. In our study, the ADC values were very accurate when a threshold value of 2.30×10^{-3} mm^2/s was used, correctly categorizing 21 (55%) of 38 hemangiomas, and missing no other hypervascular liver lesions with a sensitivity of 55% (CI, 38%-71%), a specificity of 100% (CI, 97%-100%), a positive predictive value of 100% (CI, 81%-100%), and a negative predictive value of 89% (CI, 83%-94%). A threshold of 2.00×10^{-3} mm^2/s included 29 of 38 hemangiomas, but misclassified 4 NET, 1 HCC, and 1 FNH, if only the ADC values were considered in the diagnosis, with a sensitivity of 76% (CI, 59%-88%), a specificity of 96% (CI, 91%-98%), a positive predictive value of 83% (CI, 66%-93%), and a negative predictive value of 94% (CI, 88%-97%). All lesions with an ADC value below 1.17×10^{-3} mm^2/s were malignant (Fig. 5).

In our study, we included both typical hemangiomas and atypical hemangiomas. Atypical hemangiomas mimic other malignant liver lesions and are therefore difficult to characterize. However, atypical hemangiomas were not statistically different from atypical hemangiomas in ADC values ($P = 0.99$). Our results are in line with previous studies, which concluded that DW MR imaging is useful in the diagnosis and differentiation of focal hepatic lesions, such as distinguishing cavernous hemangioma from hepatic cysts and hepatic abscess from cystic or necrotic tumor.[10,48-50] To our knowledge, however, this study was the first to use ROC analysis in assessing DW MR imaging.

This study has several limitations. First, it was a retrospective study. However, readers were blinded to the diagnosis, and there was extended follow-up (up to 2 years) to confirm the diagnosis. Second, not all lesions were histopathologically verified, because this is not usually clinically appropriate. In typical cases, histopathology is not needed to confirm the diagnosis of benign lesions. In HCC, typical imaging findings and a markedly raised α-fetoprotein level (>400) can be considered diagnostic. Third, we did not include hepatic adenomas in our study; however, we feel that this is of less clinical importance, because they are very rare and they may contain fat and are associated with a history of oral contraceptives.[51] In addition, we only included NET because they are typically hypervascular, and therefore may represent all other

hypervascular liver metastases. Last, the ADC values generated in this study are equipment-specific and may not be applicable to different vendors and various *b* values that may be used. Additional studies are warranted to verify these findings using various *b* values and different MR units.

CONCLUSIONS

We conclude that DW MR imaging and ADC maps have a potential role in the differentiation of typical and atypical hemangiomas from other hypervascular liver lesions. They provide fast and quantifiable information, independent of contrast dynamics. This information can potentially be useful when overlap between different lesions on conventional MR imaging exists.

REFERENCES

1. Le Bihan D, Breton E, Lallemand D, et al. MR imaging of intravoxel incoherent motions: application to diffusion and perfusion in neurologic disorders. Radiology 1986;161:401–407. [PubMed: 3763909]
2. Le Bihan D, Breton E, Lallemand D, et al. Separation of diffusion and perfusion in intravoxel incoherent motion MR imaging. Radiology 1988;168:497–505. [PubMed: 3393671]
3. Moffat BA, Chenevert TL, Lawrence TS, et al. Functional diffusion map: a noninvasive MRI biomarker for early stratification of clinical brain tumor response. Proc Natl Acad Sci U S A 2005;102:5524–5529. [PubMed: 15805192]
4. Moffat BA, Chenevert TL, Meyer CR, et al. The functional diffusion map: an imaging biomarker for the early prediction of cancer treatment outcome. Neoplasia 2006;8:259–267. [PubMed: 16756718]
5. Toshikuni N, Takagi S, Morii K, et al. Education and imaging. Hepatobiliary and pancreatic: calcified cavernous hemangiomas in the liver. J Gastroenterol Hepatol 2006;21:1626. [PubMed: 16928228]
6. Taouli B, Vilgrain V, Dumont E, et al. Evaluation of liver diffusion isotropy and characterization of focal hepatic lesions with two single-shot echo-planar MR imaging sequences: prospective study in 66 patients. Radiology 2003;226:71–78. [PubMed: 12511671]
7. Kamel IR, Bluemke DA, Eng J, et al. The role of functional MR imaging in the assessment of tumor response after chemoembolization in patients with hepatocellular carcinoma. J Vasc Interv Radiol 2006;17:505–512. [PubMed: 16567675]
8. Moteki T, Horikoshi H. Evaluation of hepatic lesions and hepatic parenchyma using diffusion-weighted echo-planar MR with three values of gradient *b*-factor. J Magn Reson Imaging 2006;24:637–645. [PubMed: 16888790]
9. Nasu K, Kuroki Y, Nawano S, et al. Hepatic metastases: diffusion-weighted sensitivity-encoding versus SPIO-enhanced MR imaging. Radiology 2006;239:122–130. [PubMed: 16493012]
10. Quan XY, Sun XJ, Yu ZJ, et al. Evaluation of diffusion weighted imaging of magnetic resonance imaging in small focal hepatic lesions: a quantitative study in 56 cases. Hepatobiliary Pancreat Dis Int 2005;4:406–409. [PubMed: 16109526]
11. Karhunen PJ. Benign hepatic tumours and tumour like conditions in men. J Clin Pathol 1986;39:183–188. [PubMed: 3950039]
12. Semelka RC, Sofka CM. Hepatic hemangiomas. Magn Reson Imaging Clin N Am 1997;5:241–253. [PubMed: 9113674]
13. Nelson RC, Chezmar JL. Diagnostic approach to hepatic hemangiomas. Radiology 1990;176:11–13. [PubMed: 2191359]
14. Quinn SF, Benjamin GG. Hepatic cavernous hemangiomas: simple diagnostic sign with dynamic bolus CT. Radiology 1992;182:545–548. [PubMed: 1732978]
15. Semelka RC, Brown ED, Ascher SM, et al. Hepatic hemangiomas: a multi-institutional study of appearance on T_2-weighted and serial gadolinium-enhanced gradient-echo MR images. Radiology 1994;192:401–406. [PubMed: 8029404]
16. Soyer P, Dufresne AC, Somveille E, et al. Hepatic cavernous hemangioma: appearance on T_2-weighted fast spin-echo MR imaging with and without fat suppression. AJR Am J Roentgenol 1997;168:461–465. [PubMed: 9016227]

17. Moody AR, Wilson SR. Atypical hepatic hemangioma: a suggestive sonographic morphology. Radiology 1993;188:413–417. [PubMed: 8327687]
18. Yamashita Y, Hatanaka Y, Yamamoto H, et al. Differential diagnosis of focal liver lesions: role of spin-echo and contrast-enhanced dynamic MR imaging. Radiology 1994;193:59–65. [PubMed: 8090922]
19. Mitsudo K, Watanabe Y, Saga T, et al. Nonenhanced hepatic cavernous hemangioma with multiple calcifications: CT and pathologic correlation. Abdom Imaging 1995;20:459–461. [PubMed: 7580785]
20. Jang HJ, Kim TK, Lim HK, et al. Hepatic hemangioma: atypical appearances on CT, MR imaging, and sonography. AJR Am J Roentgenol 2003;180:135–141. [PubMed: 12490492]
21. Albrecht T, Hohmann J, Oldenburg A, et al. Detection and characterisation of liver metastases. Eur Radiol 2004;14(suppl 8):P25–P33. [PubMed: 15700330]
22. Braga L, Semelka RC, Danet IM, et al. Liver metastases from unknown primary site: demonstration on MR images. Magn Reson Imaging 2003;21:871–877. [PubMed: 14599537]
23. Chung JJ, Kim MJ, Kim KW. Mangafodipir trisodium-enhanced MRI for the detection and characterization of focal hepatic lesions: is delayed imaging useful? J Magn Reson Imaging 2006;23:706–711. [PubMed: 16565954]
24. Elsayes KM, Narra VR, Yin Y, et al. Focal hepatic lesions: diagnostic value of enhancement pattern approach with contrast-enhanced 3D gradient-echo MR imaging. Radiographics 2005;25:1299–1320. [PubMed: 16160113]
25. Namasivayam S, Martin DR, Saini S. Imaging of liver metastases: MRI. Cancer Imaging 2007;7:2–9. [PubMed: 17293303]
26. Namasivayam S, Salman K, Mittal PK, et al. Hypervascular hepatic focal lesions: spectrum of imaging features. Curr Probl Diagn Radiol 2007;36:107–123. [PubMed: 17484954]
27. Sahani DV, Kalva SP. Imaging the liver. Oncologist 2004;9:385–397. [PubMed: 15266092]
28. Hosch WP, Schmidt SM, Plaza S, et al. Comparison of CT during arterial portography and MR during arterial portography in the detection of liver metastases. AJR Am J Roentgenol 2006;186:1502–1511. [PubMed: 16714637]
29. Seltzer SE, Getty DJ, Pickett RM, et al. Multimodality diagnosis of liver tumors: feature analysis with CT, liver-specific and contrast-enhanced MR, and a computer model. Acad Radiol 2002;9:256–269. [PubMed: 11887942]
30. Tomemori T, Yamakado K, Nakatsuka A, et al. Fast 3D dynamic MR imaging of the liver with MR SmartPrep: comparison with helical CT in detecting hypervascular hepatocellular carcinoma. Clin Imaging 2001;25:355–361. [PubMed: 11682296]
31. Ito K, Mitchell DG, Outwater EK, et al. Hepatic lesions: discrimination of nonsolid, benign lesions from solid, malignant lesions with heavily T_2-weighted fast spin-echo MR imaging. Radiology 1997;204:729–737. [PubMed: 9280251]
32. Baker LL, Kucharczyk J, Sevick RJ, et al. Recent advances in MR imaging/spectroscopy of cerebral ischemia. AJR Am J Roentgenol 1991;156:1133–1143. [PubMed: 2028855]
33. Schaefer PW, Grant PE, Gonzalez RG. Diffusion-weighted MR imaging of the brain. Radiology 2000;217:331–345. [PubMed: 11058626]
34. Tsuruda JS, Chew WM, Moseley ME, et al. Diffusion-weighted MR imaging of extraaxial tumors. Magn Reson Med 1991;19:316–320. [PubMed: 1881321]
35. Muller MF, Prasad P, Siewert B, et al. Abdominal diffusion mapping with use of a whole-body echo-planar system. Radiology 1994;190:475–478. [PubMed: 8284402]
36. Kim T, Murakami T, Takahashi S, et al. Diffusion-weighted single-shot echoplanar MR imaging for liver disease. AJR Am J Roentgenol 1999;173:393–398. [PubMed: 10430143]
37. Catasca JV, Mirowitz SA. T_2-weighted MR imaging of the abdomen: fast spin-echo vs conventional spin-echo sequences. AJR Am J Roentgenol 1994;162:61–67. [PubMed: 8273691]
38. Choi BI, Han MC, Kim CW. Small hepatocellular carcinoma versus small cavernous hemangioma: differentiation with MR imaging at 2.0 T. Radiology 1990;176:103–106. [PubMed: 2162066]
39. Mitchell DG. Fast MR imaging techniques: impact in the abdomen. J Magn Reson Imaging 1996;6:812–821. [PubMed: 8890021]

40. Saini S, Reimer P, Hahn PF, et al. Echoplanar MR imaging of the liver in patients with focal hepatic lesions: quantitative analysis of images made with various pulse sequences. AJR Am J Roentgenol 1994;163:1389–1393. [PubMed: 7992735]
41. Yu JS, Kim KW, Park MS, et al. Hepatic cavernous hemangioma in cirrhotic liver: imaging findings. Korean J Radiol 2000;1:185–190. [PubMed: 11752953]
42. Asbach P, Klessen C, Koch M, et al. Magnetic resonance imaging findings of atypical focal nodular hyperplasia of the liver. Clin Imaging 2007;31:244–252. [PubMed: 17599618]
43. Parkin DM, Bray F, Ferlay J, et al. Global cancer statistics, 2002. CA Cancer J Clin 2005;55:74–108. [PubMed: 15761078]
44. Kamel IR, Bluemke DA. MR imaging of liver tumors. Radiol Clin North Am 2003;41:51–65. [PubMed: 12630685]
45. Brancatelli G, Federle MP, Grazioli L, et al. Hepatocellular carcinoma in noncirrhotic liver: CT, clinical, and pathologic findings in 39 U.S. residents. Radiology 2002;222:89–94. [PubMed: 11756710]
46. Winston CB, Schwartz LH, Fong Y, et al. Hepatocellular carcinoma: MR imaging findings in cirrhotic livers and noncirrhotic livers. Radiology 1999;210:75–79. [PubMed: 9885590]
47. Sun XJ, Quan XY, Huang FH, et al. Quantitative evaluation of diffusion-weighted magnetic resonance imaging of focal hepatic lesions. World J Gastroenterol 2005;11:6535–6537. [PubMed: 16425430]
48. Chan JH, Tsui EY, Luk SH, et al. Diffusion-weighted MR imaging of the liver: distinguishing hepatic abscess from cystic or necrotic tumor. Abdom Imaging 2001;26:161–165. [PubMed: 11178693]
49. Ichikawa T, Haradome H, Hachiya J, et al. Diffusion-weighted MR imaging with a single-shot echoplanar sequence: detection and characterization of focal hepatic lesions. AJR Am J Roentgenol 1998;170:397–402. [PubMed: 9456953]
50. Namimoto T, Yamashita Y, Sumi S, et al. Focal liver masses: characterization with diffusion-weighted echo-planar MR imaging. Radiology 1997;204:739–744. [PubMed: 9280252]
51. Brancatelli G, Federle MP, Vullierme MP, et al. CT and MR imaging evaluation of hepatic adenoma. J Comput Assist Tomogr 2006;30:745–750. [PubMed: 16954922]

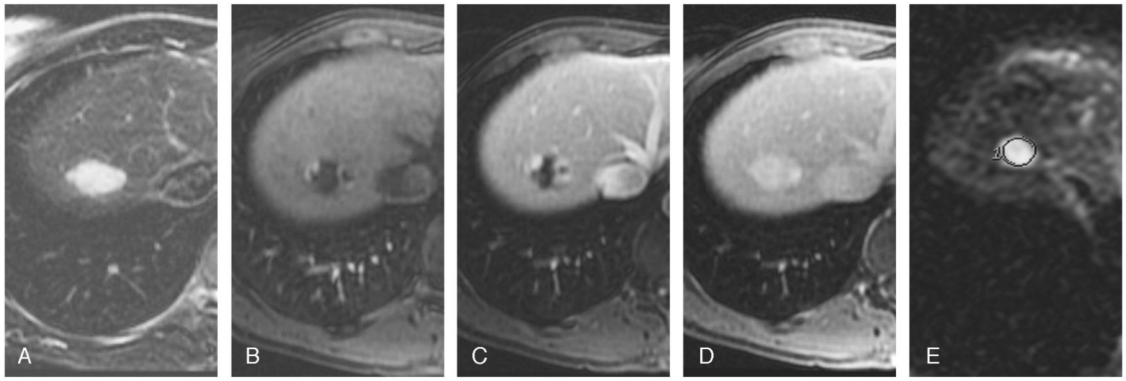

FIGURE 1.

Typical hemangioma in a 41-year-old woman. T_2-weighted image (T_R/T_E, 5000:100 milliseconds) with fat suppression shows a hyperintense lesion in the right lobe (A). Transverse dynamic fat-suppressed T_1-weighted MR images (T_R/T_E, 5.1:1.2 milliseconds) of this lesion show peripheral nodular enhancement in the hepatic arterial phase (B), centripetal enhancement in the portal venous phase (C), progressing into complete uniform filling in the delayed phase (D). Diffusion-weighted image (b = 500; T_R/T_E, 6500:110 milliseconds) shows a bright lesion with an ADC value of 2.14×10^{-3} mm^2/s (E).

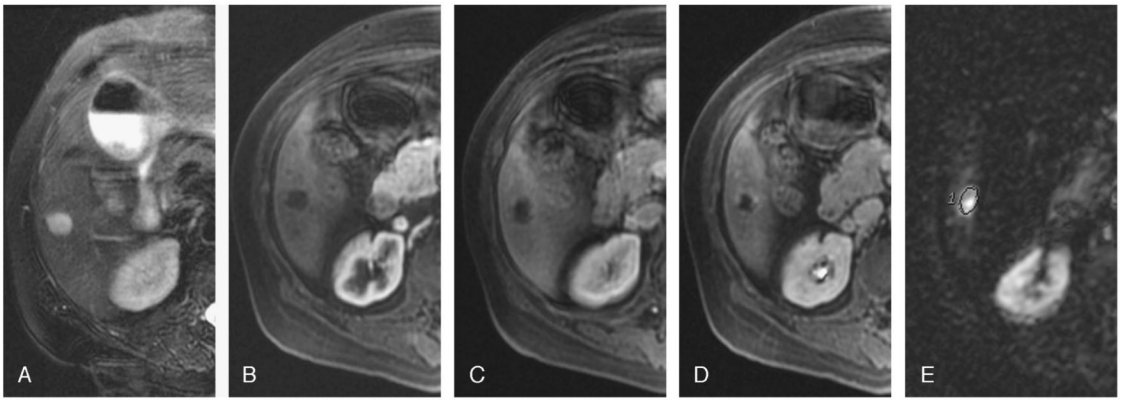

FIGURE 2.

Atypical hemangioma in a 71-year-old man. T_2-weighted images (T_R/T_E, 5000:100 milliseconds) with fat suppression show a hyperintense lesion in the right lobe (A). Transverse dynamic fat-suppressed T_1-weighted MR images (T_R/T_E, 5.1:1.2 milliseconds) of this lesion after contrast administration show no enhancement in the arterial (B) and venous (C) phases and minimal peripheral nodular in the delayed phase (D). Diffusion-weighted MR image (b = 500; T_R/T_E, 6500:110 milliseconds) shows a bright lesion (E). The ADC value was 2.00×10^{-3} mm^2/s for this lesion. The lesion remained stable for 2 years.

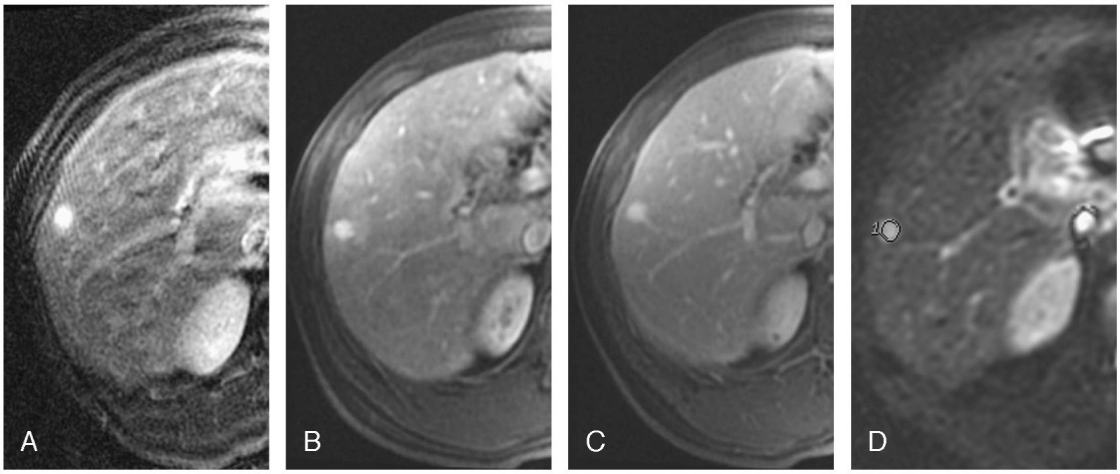

FIGURE 3.

Atypical hemangioma in a 42-year-old man. T_2-weighted images (T_R/T_E, 5000:100 milliseconds) with fat suppression show a hyperintense lesion in the right lobe (A). Transverse dynamic fat-suppressed T_1-weighted MR image (T_R/T_E, 5.1:1.2 milliseconds) of this lesion shows flash filling in the arterial phase (B) and follows the blood pool in the portal venous phase (C). Diffusion-weighted MR image (b = 500; T_R/T_E, 6500:110 milliseconds) shows a bright lesion (D). The ADC value was 3.08×10^{-3} mm^2/s for this hemangioma.

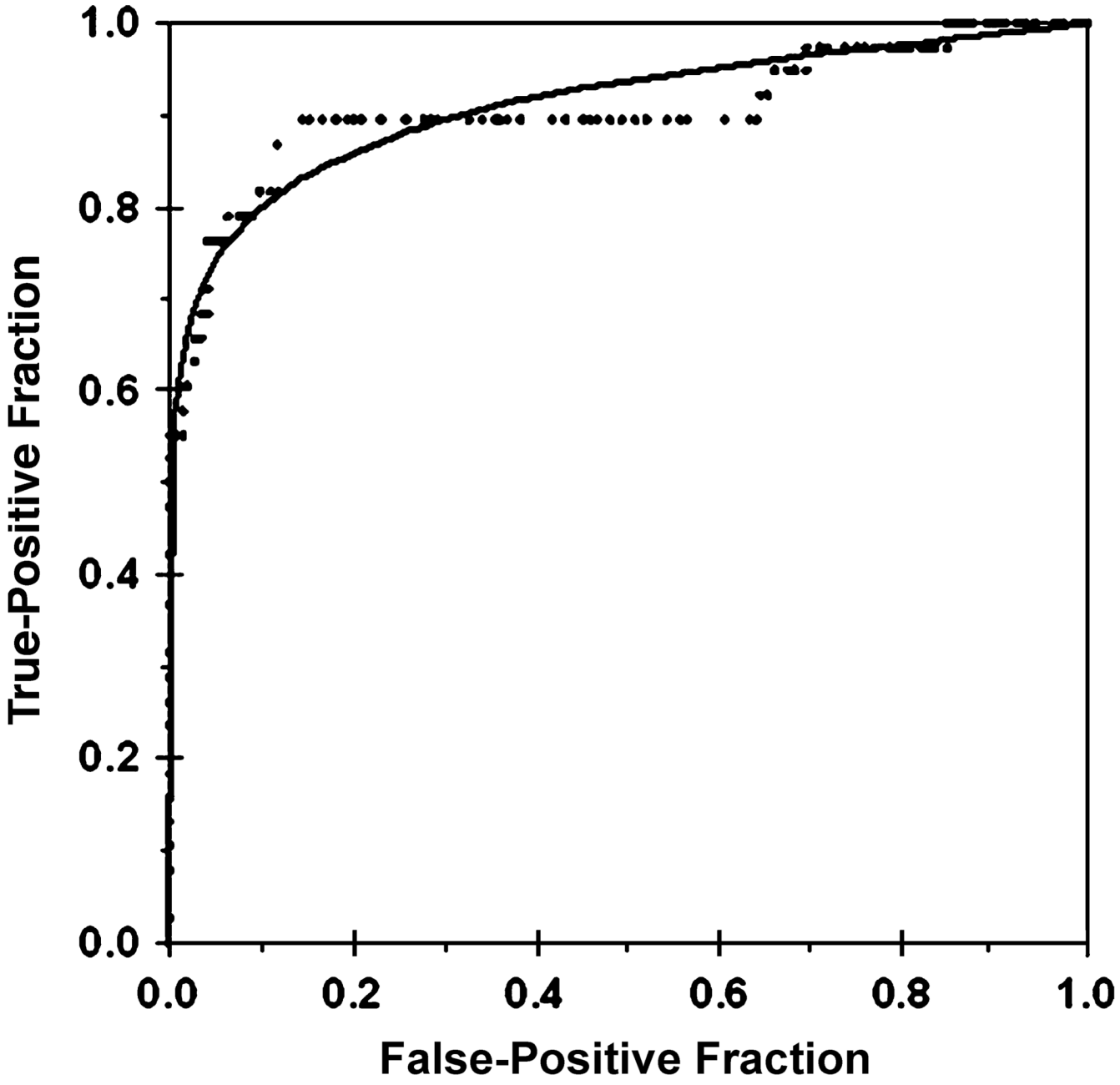

FIGURE 4.
Receiver operating characteristic curve and fitted ROC curve with an area under the ROC curve of 0.91.

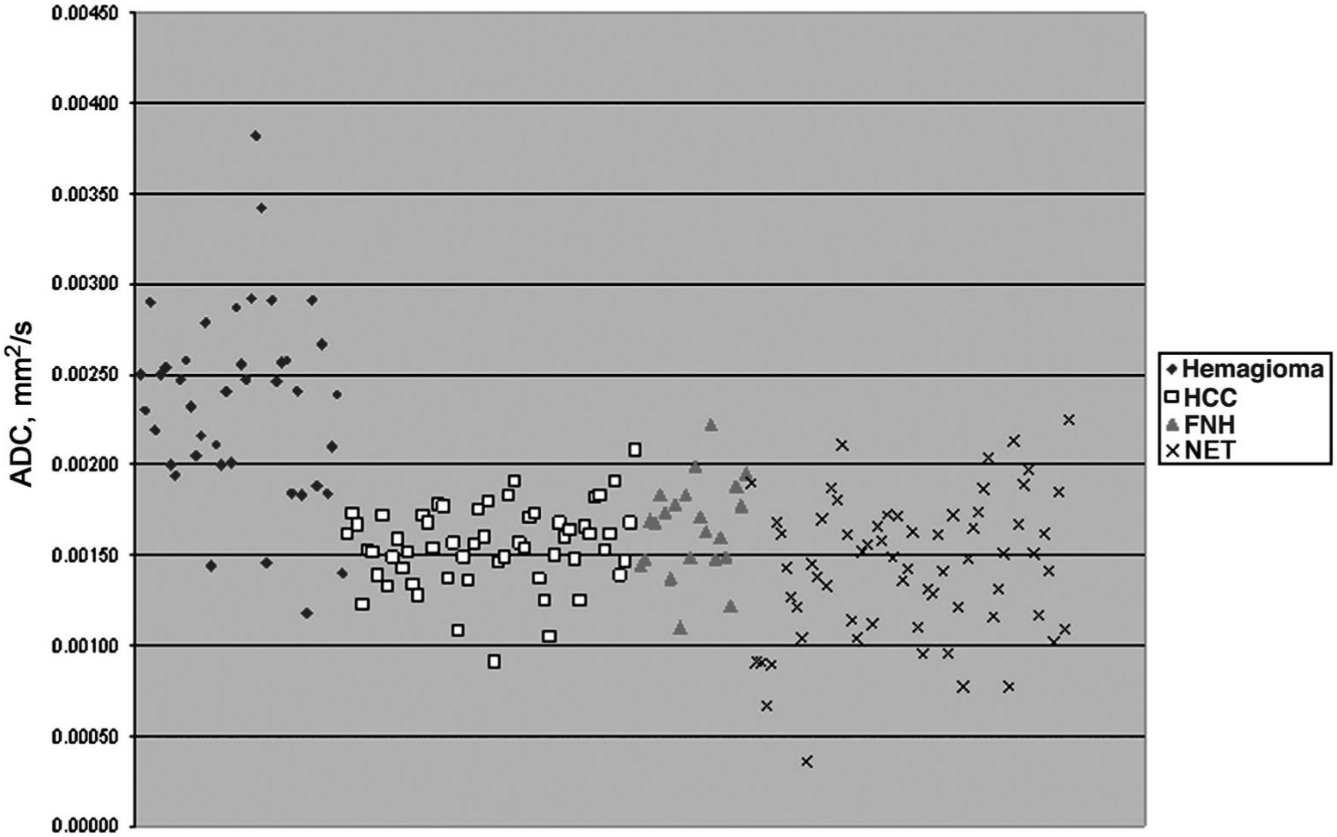

FIGURE 5.
Scatterplot of the ADC values of malignant and benign focal hepatic lesions obtained with DW MR imaging.

TABLE 1

Patient Demographics

Characteristics	Value
No. patients	117
Age, mean (range), yrs	55 (14-87)
Sex, male/female	68/49
No. lesions, mean (range)	1.5 (1-5)
Size of lesions, mean (range), cm	5.3 (1.0-17.8)
Hemangioma	3.4 (1.0-12.0)
HCC	6.7 (1.5-17.8)
FNH	4.2 (1.0-9.4)
NET	5.6 (2.0-17.0)

TABLE 2

Signal Intensity of the Lesions Relative to the Surrounding Liver Parenchyma on Diffusion-Weighted MR Images (*b* = 500)

	Signal Intensity		
Diagnosis, No. Lesions	**Very Hyperintense**	**Slightly Hyperintense**	**Isointense**
Hemangioma, n = 38	38	0	0
HCC, n = 58	10	45	3
FNH, n = 22	0	20	2
NET, n = 64	63	0	1

TABLE 3

Apparent Diffusion Coefficient Values (mm^2/s) of the Lesions

Diagnosis	Mean	SD	*P* (Compared to Hemangioma)
Hemangioma	2.29×10^{-3}	5.1×10^{-4}	NA
Typical	2.29×10^{-3}	5.6×10^{-4}	
Atypical	2.29×10^{-3}	3.9×10^{-4}	
HCC	1.55×10^{-3}	2.2×10^{-4}	<0.001
Cirrhotic	1.55×10^{-3}	2.4×10^{-4}	<0.001
Noncirrhotic	1.57×10^{-3}	2.1×10^{-4}	<0.001
FNH	1.65×10^{-3}	2.6×10^{-4}	<0.001
NET	1.43×10^{-3}	3.9×10^{-4}	<0.001

NA indicates not applicable.